MICROSTRUCTURE AND PROPERTIES OF HYBRID COAL GANGUE-BASED ALKALI-ACTIVATED CEMENT

Bruna J. FRASSON (1), Malik CHERIAF (2) and Janaíde C. ROCHA (2)

(1) Civil Engineering, CTC, Federal University of Santa Catarina, Brazil

(2) Department of Civil Engineering, CTC, Federal University of Santa Catarina, Brazil

Abstract

Addition of Portland cement in low-calcium aluminosilicate-based alkali-activated materials can provide rapid hardening at room temperature, thus modifying microstructure and mechanical properties. In the present study, the effect of Portland cement addition on alkali-activated materials, cured at room temperature, was analysed by mechanical strength test, FT-IR and electrochemical impedance spectroscopy. The results showed samples hardening at room temperature after 24 hours and compressive strength of 26 MPa (7 days) for 5% of OPC addition. Hybrid alkali-activated cements presented higher sorptivity and lower electrical resistance than alkali-activated cement without OPC addition which can be related to more connected pores. The analysis of EIS spectrum highlights continued formation of microstructure over the ages of alkali-activated cement and can be related to mechanical properties and sorptivity.

Keywords: hybrid, alkali-activated, coal gangue, compressive strength, sorptivity.

1. INTRODUCTION

Synthesis of Alkali-activated binders (AAM) occurs by chemical reaction between aluminosilicate sources and alkaline reagents. The process consists basically of dissolution, agglomeration and polymerization [1], thus amorphous aluminosilicate gel (Me-A-S-H) is the main reaction product [2]. Low-calcium aluminosilicate-AAM generally presents slow hardening and long setting time at room temperature, hence thermal cure is required to accelerate the reaction process [3].

Portland cement addition (OPC) in AAM is an alternative to accelerate chemical reaction and provide hardening at room temperature, therefore, forming hybrid cements. OPC addition increases internal temperature during reaction [4] and provides formation of complex microstructure, where N-A-S-H and C-A-S-H precipitate [5]. Industrial by-products and calcined clay, such as fly ash, slag and metakaolin are the main aluminosilicates studied [1]. Mining wastes red mud [2] and coal gangue [6, 7] have been used as aluminosilicate to produce AAM.

In Brazil, coal mining industry in southern region, extracts around 6 million tons per year [8]. However, about 60% are impurities generated by the washing process. Fine wastes go through neutralization and decantation processes, forming sludge from decantation basin (CS). Coal mining wastes contain Al_2O_3, SiO_2 and low Fe_2O_3 [9, 10, 11], in mineralogical phases such as quartz and kaolinite. Dehydroxylation of kaolinite occurs at calcination temperature between 500ºC and 700ºC making it more reactive [9] and calcination also provides the burn organic. However, during calcination, CO_2 and SO_2 are released, and pyrite transformation is the main cause of SO_2 release [12].

Microstructure development can be observed by electrical parameters, obtained by means of electrochemical impedance spectroscopy (EIS). There is little research for the use of EIS, in alkali-activated materials, the main analyzes are related to reaction kinetics [13, 14], transport properties [15, 16] and microstructure development [17].

This study aimed to analyze the effect of Portland cement addition in microstructure and mechanical properties of hybrid alkaline cements by means of compressive strength, FT-IR and electrochemical impedance technique.

2. MATERIALS AND METHODS

2.1 Materials

The coal sludge (CS) was used as aluminosilicate, oven dried at 100°C for 24 hours and ball milled for 30 minutes. Coal sludge was calcined at 700°C for 1 hour and then designated as CST. Early high strength Portland cement replaced wastes in 5 wt% and 10 wt%. Chemical and mineralogical composition of materials were performed in a previous work [18]. However, calcination of CS provided reduction of volatile material, sulfur and kaolinite dehydroxylation.

Sodium hydroxide (97% Na_2O) and sodium silicate (12.7% Na_2O, 30.4% SiO_2 and 56.9% H_2O) were used to prepare alkaline solution (AS). NaOH (solid) was dissolved in sodium silicate to obtain the SA with a silica modulus (SiO_2 / Na_2O) of 1.5.

2.2 Methods

Alkali-activated cements were prepared by pre-mixing OPC and wastes, then added to AS at a 1:1 mass ratio, the water to binder ratio was 0.75. Cylindrical samples of 2 x 4 cm (diameter x height) were filled, hermetically sealed and cured at room temperature (25°C), after 24 hours were demolded and sealed with PVC film. Table 1 shows binders' compositions, the CST-0 was heat-cured in oven at 50°C for hours.

Compressive strength test was performed at 7 and 28 days in Instron press with 50 kN static load cell and at 7000 N/min loading speed. Fragments of cements were submerged in acetone for 24 hours, filtered, oven dried at 50°C for 24 hours and grounded to particles less than 150 μm. FT-IR spectra were obtained in Agilent Carry 600, averaging 32 scans, in transmission mode, ranging from 4000cm $^{-1}$ to 400cm $^{-1}$, and 4cm $^{-1}$ resolution, the powders were prepared with KBr.

Alkali-activated hybrid mortars were prepared for EIS and capillary water absorption tests. Mortars were prepared by mixing the binders with sand to binder ratio of 3 (mass). Cylindrical samples of 5 x 10 cm (diameter x height) were filled, sealed and cured at room temperature, except the CST-0, which was thermally cured. Electrochemical Impedance Spectroscopy (EIS) was performed in 100 MHz bandwidth digital oscilloscope (Tektroniz

TDS 3014C), function generator (AFG 3102) and current gauges (P6022). The data was measured at 7, 14 and 21 days then analyzed in the EISA software [19] using Complex Nonlinear Least Squares – CNLS algorithm. ErroX was determined by simplex method [20]. Capillary water absorption test was performed at 28 days, the samples were dried in oven at 50° C for 72 hours before the water absorption test, that was performed over 24 hours, as described by Santos et al [21].

Table 1: Mix proportions and molar ratio

Designation	Waste (g)	OPC (g)	SiO_2/Al_2O_3 (mol/mol)	Na_2O/Al_2O_3 (mol/mol)	% CaO
CST-0	100	0	3.35	0.99	1.05
CST-5	95	5	3.40	1.04	6.15
CST-10	90	10	3.46	1.10	11.25
CS-5	95	5	4.94	3.09	7.86
CS-10	90	10	5.11	3.27	12.87

3. RESULTS AND DISCUSSIONS

3.1 Cements compressive strength and microstructure formation

Fig. 1 shows visual aspect of cements at 28 days, efflorescence appears in CS-systems which is related to presence of free alkaline cation (Na^+) and lower reactivity of coal sludge. Alkaline cation percolate through connected pores and reacts with CO_2, yielding sodium carbonates on material surface. Mechanical strength of alkali-activated cement is shown in Fig. 2, in general there is an increase in compressive strength over the ages, except for CST-10.

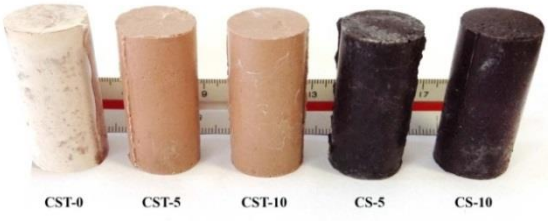

Figure 1: Alkali-activated cements at 28 days

Hardening and compressive strength of alkali-activated cements cured in room temperature are influenced by OPC addition. CST-5 and CST-10 present hardening at 24 hours and increase of 45% and 108% respectively in compressive strength over CST-0. Reaction kinetics and microstructure formation can be accelerated by addition of calcium sources, which implies strength development [7] and an increase of stiffness. Compressive strength of CS-systems is 40% lower than CST-systems and it was not influenced by different OPC addition. CS mineralogical and chemical composition may affect microstructure development and the mechanical properties.

FT-IR spectra of aluminosilicates materials and AAM at 28 days are presented in Fig. 3. Vibration bands at 3620 cm^{-1} to 3696 cm^{-1} related to presence of hydroxyl groups and at 1033 cm^{-1} and 1016 cm^{-1} of Si-O bonds, and 912 cm^{-1} 1538 cm^{-1} of Al-OH and Si-O-Al respectively, point kaolinite content in CS. Kaolinite dehydroxylation and break of Al-OH and Si-O-Al were observed from CST-spectra, which was evidenced by the disappearance of hydroxyl bands and the absence of 912 cm^{-1} and 538 cm^{-1} [22].

Alkaline activation alters the main vibration band (1000-1100 cm^{-1}) to lower frequencies, related to asymmetric T-O vibration (T: Si or Al), amorphous aluminosilicate gel is evidenced by changes in this vibration band range [23]. In CST systems the peak shifts from 1052 cm^{-1} to 1027 cm^{-1}, 1024 cm^{-1} and 1016 cm^{-1} for CST, CST-0, CST-5 and CST-10 respectively (Fig. 3b). OPC addition provides slight displacement of the main band of CST-5 (-3 cm^{-1}) and CST-10 (-11 cm^{-1}) compared to CST-0. Between CS-5 and CS-10 no changes were observed which is in agreement to the mechanical strength.

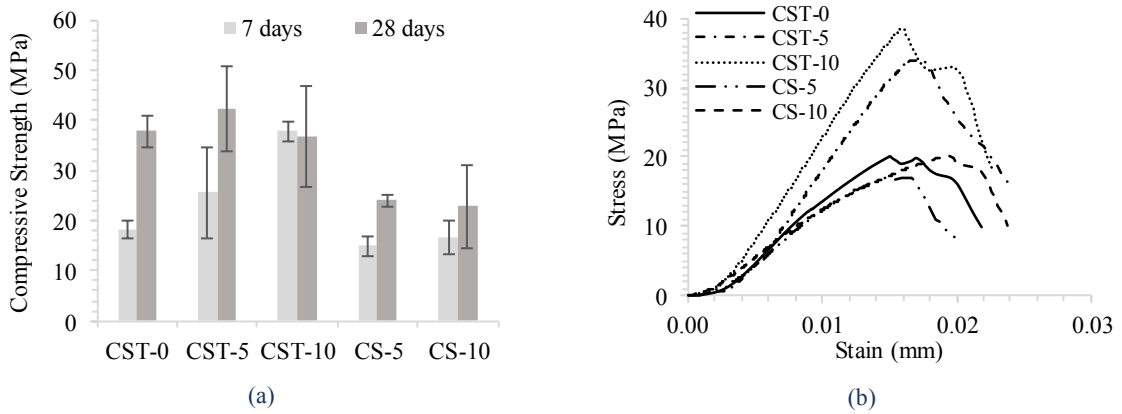

Figure 2: Alkali-activated cements (a) compressive strength; (b) stress x strains plot at seven days.

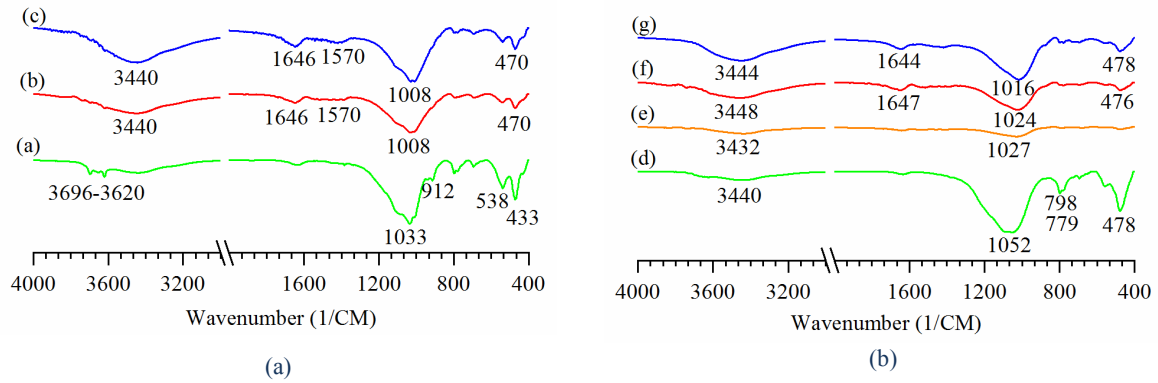

Figure 3: FT-IR spectrogram of aluminosilicate and alkali-activated cements (a) CS-powder; (b) CS-5; (c) CS-10; (d) CST-powder; (e) CST-0; (f) CST-5; (g) CST-10.

3.2 Mortar impedance spectroscopy and sorptivity

Electrochemical impedance spectroscopy presents a complex graph, which the abscissa axis is related to the real component and the ordinate to imaginary. Electrical parameters and equivalent electrical circuits were obtained by means of EISA software. Voight type reactive circuit and blocking circuit were simulated according to the scheme of Fig.4. The complex equations are present below. Wherein Z: Electrochemical Impedance (Ω), R_1: electrolyte/ohmic Resistance (Ω), R_2: charge transfer Resistance (Ω), ω is frequency (Hz) and C_p: double layer Capacitance (Farad).

$$Z = R_1 - [1/(i\omega C_p)] - \text{Blocking circuit} \quad (1)$$

$$Z = R_1 + 1/[(i\omega C_p) + 1/R_2] - \text{Voight circuit} \quad (2)$$

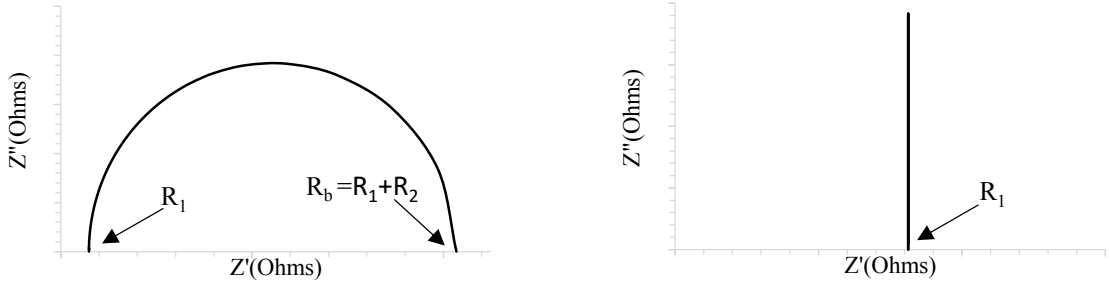

Figure 4: Simulated (a) Reactive circuit – Voight; (b) blocking circuit;

Nyquist arc increases over the time for all CST mortars and indicates continuous microstructure formation, which is correlated to the mechanical strength increase. Electrical parameters are shown in Table 2 and complex plots for all sample in the Fig. 5. CST-0 electrical resistance parameter (R_1 and R_2) is higher than other mortars at all ages analyzed. CST-0 electrical parameters and Nyquist plot (Fig. 5a) indicates acceleration of reaction mechanisms due to thermal cure (50˚C for 24 hours), which will consume alkaline ions and evaporate free water.

CST-5 presents at seven days a blocking circuit (Eq. 1 and Fig. 5b), although at 14 and 21 days the Nyquist arc is formed, related to the Voight circuit (Eq. 2), and suggests a delay in the reaction process. CST-10 presents at seven days Nyquist arc formation (reactive circuit Eq. 2 and Fig. 5c), and increase in the electrical resistance over the time. Portland cement content influenced the impedance spectra and the R_2, which may relate to the quick reaction provided by the hydration of OPC particles.

However, at 21 days CST-5 and CST-10 show similar electrical parameters (R_1, R_2 and C_p). These analyzes may be correlated to results of mechanical resistance, where at seven days is higher for CST-10 than for CST-5, but similar at 28 days. Reaction rates at early ages (seven ages) influences mortars electrical parameters and the reaction kinetics are affected by OPC addition, leading to hardening and microstructure formation. Therefore, at older ages (more than 7 days) electrical parameters are controlled by aluminosilicate chemical reactions [24].

Table 2: Electrical parameters and sorptivity results

Mortar	Age	R_1 (Ω)	R_2 (Ω)	C_p (pF)	Error Simplex	Sorptivity (μm/s$^{1/2}$)
CST-0	7 days	215.6	2406.4	101.18	14.30	5.6 [18]
	14 days	225.9	2826.7	74.46	16.21	
	21 days	294.1	3841.9	60.07	18.92	
CST-5	7 days	326.3	-	-	0.76	9.48
	14 days	393.1	46.4	1410.30	1.72	
	21 days	364.1	750.9	111.06	5.62	
CST-10	7 days	286.4	559.3	99.52	6.64	8.57
	14 days	310.6	758.9	95.99	7.25	
	21 days	409.9	853.4	123.54	5.64	
CS-10	7 days	161.1	-	-	12.74	4.28
	14 days	140.7	-	-	0.35	
	21 days	138.0	-	-	0.17	

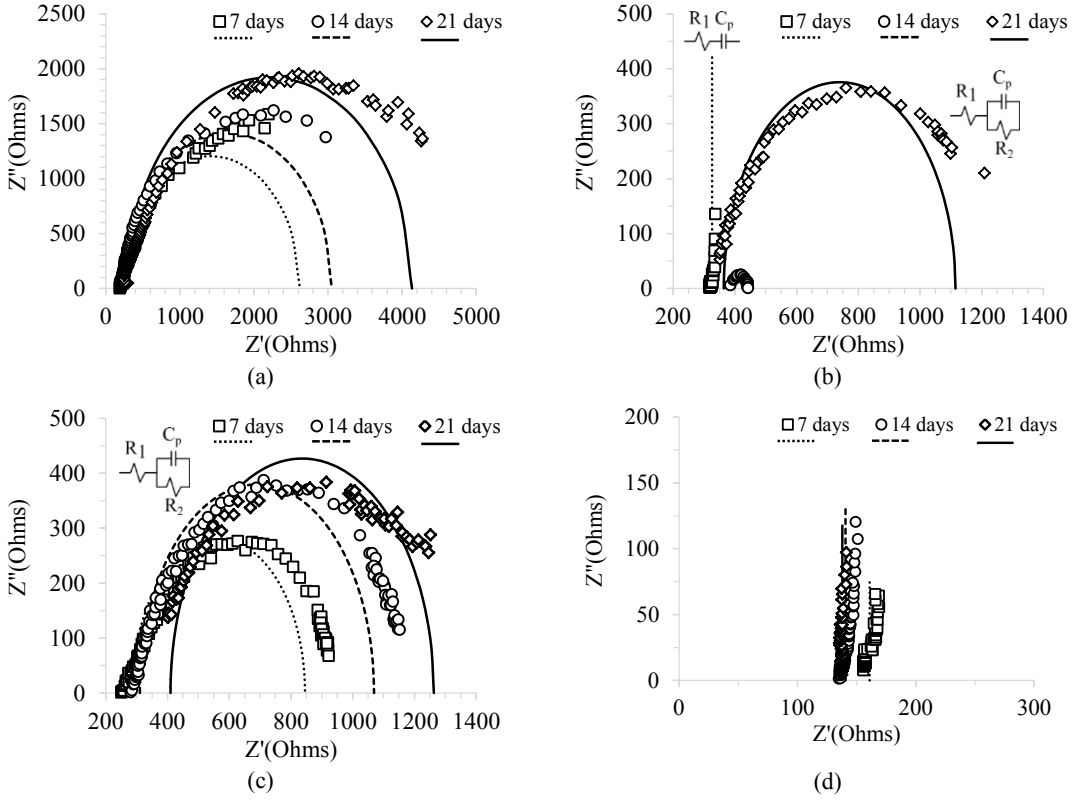

Figure 5: Nyquist plot to mortars (a) CST-0; (b) CST-5; (c) CST-10; (d) CS-10.

Mortar sorptivity are present in Table 2, the results suggest higher connected pore structure for CST-10 than to CST-0 and CST-5. The results of CST-0 are presented in previous studies [18] but are included here for comparative analysis with other mortars. CST-0 was thermal cure, which allows acceleration of microstructure formation thus indicates denser microstructure, with smaller pores and a more tortuous network [24]. However, higher permeability of CST-5 and CST-10 did not influence mechanical strength; the results were similar in all CST-systems at 28 days. Sorptivity can be related to the electrical parameters, the lower sorptivity the higher electrical resistance (R_b=R_1+R_2) and the lower capacitance.

Blocking circuit are evidenced in CS-10 mortars, at test ages, and indicates ideally polarizable electrode [25]. Poor microstructure formation and high free alkaline cation can be related to this behavior, which leads to higher electrical conductivity. CS-10 presents lower sorptivity than CST-10 and CST-5; physical, chemical and mineralogical characteristics of CS may affect porous structure.

4. CONCLUSIONS

The main conclusions obtained from the experimental analyses are listed below:

- Aluminosilicate replacement for Portland cement increased compressive strength and stiffness of hybrid alkali-activated pastes at seven days. Formation of N-A-S-H as the main reaction product is evidenced by FT-IR;
- EIS highlights the continued formation of microstructure in CST systems over time. Calcium contents affected the development of the microstructure at seven days (early ages), this effect is evidenced by the formation of complex arc and the parameter of electrical resistance (R_2);
- Sorptivity was higher for hybrid mortars than for CST-0, which may be related to the formation of different microstructures. The addition of Portland cement modified porous structure and influenced the permeability; however, mechanical strength was similar at 28 days for CST-systems;
- The mortar produced with CS presents different behavior than CST; it was evidenced low microstructure formation (EIS), despite lower sorptivity than the other mortars. Complementary tests are necessary for a better understanding of the CS system.

ACKNOWLEDGEMENTS

This study was financed in part by the Coordenação de Aperfeiçoamento de Pessoal de Nível Superior - Brasil (CAPES) – Finance Code 001.

REFERENCES

[1] Provis, J. L.; Palomo, A. and Shi, C. ‘Advances in understanding alkali-activated materials’. *Cement Concrete Res.* **78**(2015)110–125.

[2] Shi, C.; Fernández-Jiménez, A. and Palomo, A. ‘New cements for the 21st century: The pursuit of an alternative to Portland cement’. *Cement Concrete Res*., **41**(2011) 750–763.

[3] Cheng, Y.; Hongqiang, M.; Hongyu, C.; Jiaxin, W.; Jing, S.; Zonghui, L. and Mingkai, Y. ‘Preparation and characterization of coal gangue geopolymers’. *Constr. Build. Mater.* **187**(2018)318–326.

[4] Garcia-Lodeiro, I.; Fernandez-Jimenez, A. and Palomo, A. ‘Hydration kinetics in hybrid binders: Early reaction stages’. *Cement Concrete Comp.*, **39**(2013)82–92, 2013.

[5] Provis, J. L.; Palomo, A. and SHI, C. 'Advances in understanding alkali-activated materials'. *Cement Concrete Res.*, **78**(2015)110–125.
[6] Cheng, Y.; Hongqiang, M.; Hongyu, C.; Jiaxin, W.; Jing, S.; Zonghui, L. and Mingkai, Y. 'Preparation and characterization of coal gangue geopolymers'. *Constr. Build. Mater.* **187**(2018)318–326.
[7] Huang, G.; Ji, Y.; Li, J.; Hou, Z. and Dong, Z. 'Improving strength of calcinated coal gangue geopolymer mortars via increasing calcium content'. *Constr. Build. Mater*. **166**(2018)760–768.
[8] Carvão Mineral - SieceSC. *Informações sobre o carvão mineral em SC.* November 2019, http://www.siecesc.com.br/siecesc/informacoes-sobre-o-carvao-mineral-em-santa-catarina.
[9] Cao, Z.; Cao, Y.; Dong, H.; Zhang, J. and Sun, C. 'Effect of calcination condition on the microstructure and pozzolanic activity of calcined coal gangue'. *Int. J. Mineral Process.* **146**(2016) 23–28.
[10] Dong, Z.; Xia, J.; Fan, C. and Cao, J. 'Activity of calcined coal gangue fine aggregate and its effect on the mechanical behavior of cement mortar'. *Constr. Build. Mater*. **100**(2015)63–69.
[11] Cheng, Y.; Hongqiang, M.; Hongyu, C.; Jiaxin, W.; Jing, S.; Zonghui, L. and Mingkai, Y. 'Preparation and characterization of coal gangue geopolymers'. *Constr. Build. Mater.* **187**(2018)318–326.
[12] Zhang, Y.; Ge, X.; Nakano, J.; Liu, L.; Wang, X.; Zhang, Z. 'Pyrite transformation and sulfur dioxide release during calcination of coal gangue'. *RSC Adv.* **4**(2014)42506-42513.
[13] Provis, J. L.; Walls, P. A. and Van Deventer, J. S. J. 'Geopolymerisation kinetics. 3. Effects of Cs and Sr salts'. *Chem. Eng. Sci.*, **63**(18)(2008)4480–4489.
[14] Mccarter, W. J.; Chrisp, T. M. and Starrs, G. 'Early hydration of alkali-activated slag: Developments in monitoring techniques'. *Cement Concrete Comp*., **21**(4)(1999) 277–283.
[15] Nguyen, Q. H.; Lorente, S.; Duhart-Barone, A. Lamotte, H. 'Porous arrangement and transport properties of geopolymers'. *Constr. Build. Mater.*, **191**(2018)853–865.
[16] Ravikumar, D. and Neithalath, N. 'An electrical impedance investigation into the chloride ion transport resistance of alkali silicate powder activated slag concretes'. *Cement Concrete Comp.*, **44**(2013)58–68
[17] Zeng, S. and Wang, J. 'Characterization of mechanical and electric properties of geopolymers synthesized using four locally available fly ashes'. *Constr. Build. Mater.*, **121**(2016)386–399.
[18] Frasson, B. J.; Pinto, R. C. A. and Rocha, J. C. 'Influence of different sources of coal gangue used as aluminosilicate powder on the mechanical properties and microstructure of alkali-activated cement'. *Mater. Construcc.* **69**(336)(2019)1-18.
[19] Bandarenka, A. S.; Ragoisha, G. A. *In progress in chemometrics research*. New York, 2005. http://www.abc.chemistry.bsu.by/vi/analyser.
[20] Keddam, M.; Takenouti, H.; Nóvoa, X. R.; Andrade, C.; Alonso, C. 'Impedance measurements on cement paste'. *Cement Concrete Res.*, **27(**8)(1997)1191–1201.
[21] Santos, F. I. G.; Rocha, J. C. and Cheriaf, M. 'Influence of bottom ash replaced natural aggregate and air-entraining agent in moisture transfer mechanisms in mortars'. *Revista Matéria.* **12**(2)(2007) 253–268.
[22] Guo, W.; Zhu, J.; Li, D.; Chen, J. and Yang, N. 'Early hydration of composite cement with thermal activated coal gangue'. *J. Wuhan University of Technology*. **25**(1)(2010)162–166.
[23] Garcia-Lodeiro, I.; Palomo, A.; Fernández-Jiménez, A. and MacPhee, D. E. 'Compatibility studies between N-A-S-H and C-A-S-H gels. Study in the ternary diagram Na2O-CaO-Al2O3-SiO 2-H2O'. *Cement Concrete Res*. **41**(9)(2011)923–931.
[24] Noushini, A. and Castel, Arnaud. 'The effect of heat-curing on transport properties of low-calcium fly ash-based geopolymer concrete'. *Constr. Build. Mater*. **112**(2016)464–477.
[25] Vladikova, Daria. 'The technique of the differential impedance analysis part i: basics of the impedance spectroscopy'. *Advanced Techniques for Energy Sources Investigation and Testing*, (2004).